

# A Floe Size Dependent Scattering Model in Two- and Three-dimensions for Wave Attenuation by Ice Floes

Michael H. Meylan<sup>a</sup>, Christopher Horvat<sup>b</sup>, Cecilia M. Bitz<sup>c</sup>, Luke G. Bennetts<sup>d</sup>

<sup>a</sup>*School of Mathematical and Physical Sciences, The University of Newcastle, Callaghan, NSW 2308, Australia*

<sup>b</sup>*Institute at Brown for Environment and Society, Brown University, Providence, RI, USA*

<sup>c</sup>*Department of Atmospheric Sciences, University of Washington, Seattle, WA, USA*

<sup>d</sup>*School of Mathematical Sciences, University of Adelaide, Adelaide, SA 5005, Australia*

---

## Abstract

Two- and three-dimensional models are proposed for ocean-wave attenuation due to scattering by ice floes in the marginal ice zone, in which the attenuation rate depends on the horizontal size of the individual floes. The scattering models are shown to reproduce the behaviour of wave attenuation over short wave periods. However, it is shown that scattering alone cannot explain the observed asymptotic dependence of attenuation at long wave periods. Based on these findings, it is proposed that attenuation models consist of a scattering component supplemented by an empirical damping term based on measurements, so that attenuation over all periods is correctly modelled. Computer code to calculate wave attenuation through a field of ice floes is provided in the supplementary material.

*Keywords:* Sea Ice, Ocean Waves, Scattering

---

## 1. Introduction

Understanding the interaction between ocean waves and the sea-ice covered ocean has applications ranging from predicting sea ice extent to safe

---

\*Corresponding author.

*Preprint submitted to Ocean Modelling*  
Email addresses: [mike.meylan@newcastle.edu.au](mailto:mike.meylan@newcastle.edu.au) (Michael H. Meylan), (Michael H. Meylan) August 20, 2021

27 navigation. Ocean waves are frequently observed to impact the sea ice cover  
28 and to be attenuated by the ice cover (Kohout et al., 2014; Meylan et al.,  
29 2014). There is evidence that ocean waves modulate sea-ice extent (Zhang  
30 et al., 2016; Bennetts et al., 2017; Boutin et al., 2018; Roach et al., 2018,  
31 2019; Bateson et al., 2020), and that attenuation of waves by sea ice protects  
32 ice shelves (Massom et al., 2018; Chen et al., 2019b).

33 A concerted effort has emerged to include and evolve the coupled repre-  
34 sentation of sea ice and ocean surface waves into large-scale models for im-  
35 proved ice–ocean physics and prediction (Bateson et al., 2020; Boutin et al.,  
36 2020; Roach et al., 2019; Dumont et al., 2011; Williams et al., 2013a,b; Hor-  
37 vat and Tziperman, 2015; Horvat et al., 2016; Williams et al., 2017; Meylan  
38 et al., 2020). This effort has been focused mainly in the marginal ice zone  
39 (MIZ), where sea ice is highly fragmented, mobile, and in contact with ocean  
40 waves. Models include a parameterisation of the wave attenuation coefficient  
41 (i.e. the exponential rate of wave attenuation over distance travelled), gener-  
42 ically written  $\alpha(A, T, h, a)$ , where  $A$  is the wave amplitude,  $T$  is wave period,  
43  $h$  is sea ice thickness, and  $a$  is the floe radius.

44 Measurements of wave attenuation by sea ice began with pioneering work  
45 by members of the Scott Polar Institute (Squire and Moore, 1980; Wad-  
46 hams et al., 1988). In recent years, technological developments have allowed  
47 more detailed measurements of wave attenuation (Kohout et al., 2014; Mey-  
48 lan et al., 2014; Doble et al., 2015; Rogers et al., 2016; Cheng et al., 2017;  
49 Meylan et al., 2018; Sutherland et al., 2018; Thomson et al., 2018; Rabault  
50 et al., 2020; Horvat et al., 2020; Rogers et al., 2020; Alberello et al., 2020)  
51 and better constraints on the form of  $\alpha$ . The data collected show the atten-  
52 uation coefficient for long-period waves (above 10 seconds) is approximately  
53 proportional to the wave period to the power of minus two, i.e.  $\alpha \sim T^{-2}$  for

54  $T > 10$  s.

55 Theoretical modelling of wave attenuation by sea ice has been the subject  
56 of parallel research advances (Squire, 2020). Models can be broadly divided  
57 into two categories: those treating sea ice as a viscous layer (Weber, 1987;  
58 Keller, 1998; Wang and Shen, 2010a; Sutherland et al., 2019; Chen et al.,  
59 2019a; Cheng et al., 2020) and those treating it as a scattering medium  
60 (Meylan et al., 1997; Kohout and Meylan, 2009; Bennetts et al., 2010; Ben-  
61 netts and Squire, 2012; Montiel et al., 2016). Viscous layer models idealise  
62 the field of floes in the MIZ as a continuum, and are intuitively applicable in  
63 the long-wavelength limit. The layer models have been extended beyond  
64 viscosity, for example, Voermans et al. (2019) considered attenuation due to  
65 turbulence. In contrast, scattering models involve a large collection of indi-  
66 vidual floes, where the standard model for wave scattering by a single floe is  
67 based on a floating elastic thin plate model, and accounts for the compliant  
68 bending of large floes while preserving the rigidity of small floes (Meylan and  
69 Squire, 1994; Meylan, 2002; Bennetts and Williams, 2010).

70 With the exception of Perrie and Hu (1996) and the recent work Meylan  
71 et al. (2020), only two-dimensional (one horizontal dimension and one depth  
72 dimension) scattering models that have been implemented in large-scale pre-  
73 diction models, and often assuming floe lengths are much larger than the  
74 wavelength to avoid artificial resonance effects (Kohout and Meylan, 2008;  
75 Williams et al., 2013a; Bennetts and Squire, 2012). Contemporary three-  
76 dimensional scattering models of wave attenuation (Peter and Meylan, 2009;  
77 Bennetts and Squire, 2009; Bennetts et al., 2010; Montiel et al., 2016) have  
78 not yet produced a formula for  $\alpha$  suitable for inclusion in large-scale models,  
79 and this is the subject of ongoing research (Meylan and Bennetts, 2018).

80 Scattering of ocean waves by ice floes only occurs when there is a momen-

81 tum exchange between the ice floe and ocean waves. In turn, the momentum  
82 exchange implies that a force is applied to the ice floe, and hence it is liable  
83 to fracture. Therefore, the effect of scattering is central to understanding ice  
84 pack break up due to waves and other processes (Kohout et al., 2016; Herman  
85 et al., 2018). After the ice pack has been broken into smaller floes, scattering  
86 is likely to have a weaker effect, especially for the long-period waves which  
87 persist far into the MIZ (Collins et al., 2015; Dolatshah et al., 2018).

88 There is clear evidence from experiments that the ice cover causes energy  
89 to be removed from waves at a much greater rate than for an ocean without  
90 an ice cover. However, there is no evidence to show what the mechanism  
91 is that removes this energy. There is evidence to suggest that it is caused  
92 by under-ice friction (Liu and Mollo-Christensen, 1988; Ardhuin et al., 2016;  
93 Boutin et al., 2018), floe collisions (Shen and Squire, 1998; Bennetts and  
94 Williams, 2015; Yiew et al., 2017), overwash (Toffoli et al., 2015; Nelli et al.,  
95 2017, 2020), or viscoelastic bending (Wang and Shen, 2010b; Mosig et al.,  
96 2015). There is also evidence that the wave action breaks the floes in a highly  
97 active breaking region (which scattering is probably dominant) until the floes  
98 are sufficiently fractured that scattering is negligible and other mechanisms  
99 then dominate the wave attenuation (Ardhuin et al., 2020). Further evidence  
100 of this can be recent results on floe breaking (Voermans et al., 2019).

101 Despite the need to model wave attenuation and sea ice fracture accu-  
102 rately, a model including all required features of attenuation is lacking. This  
103 paper proposes an open-source model that captures both the short and long-  
104 period wave attenuation through the sea-ice cover. For short periods, we  
105 use scattering theory to account for the strong attenuation of small floes,  
106 including the effect of floe size variability. For long periods we propose an  
107 extra term which is based on experimental measurements which can easily

108 be updated with additional experimental data or appropriate theory. The  
109 computer code required to run the model is provided as supplementary ma-  
110 terial.

## 111 **2. Attenuation, scattering and dissipation**

112 There is some ambiguity in the terms attenuation, scattering and dissi-  
113 pation and we want to be clear here what we mean by these words. At-  
114 tenuation is the observed decrease in wave height as it propagates through  
115 the MIZ. Scattering is the process that changes the direction of propagation  
116 without removing energy and dissipation is a process which removes wave  
117 energy. Both scattering and dissipation can lead to attenuation.

118 A critical difference between scattering and dissipation is that scattering  
119 will lead to broadening of the wave direction and eventually to an isotropic  
120 wave field (if there is no significant dissipation). This is attested to in mod-  
121 els (Montiel et al., 2016), although there is no clear observational evidence.  
122 Scattering must involve momentum exchange and hence high forces and is  
123 likely to cause fracture or melting. Scattering models have clear and straight-  
124 forward physics, which is the basis for offshore engineering and ship design  
125 and which has been well validated in laboratory experiments (Meylan et al.,  
126 2015; Montiel et al., 2013a). It is possible that scattering only plays a signif-  
127 icant role in the active breaking region, but we believe its influence is more  
128 comprehensive than this. However, we acknowledge that evidence to prove  
129 this is lacking.

## 130 **3. Wave scattering by individual ice floes**

131 The scattering model treats an ice floe as a floating, elastic plate, which  
132 behaves as a rigid body in the case of long waves or large thickness. We

133 present a simple numerical method that works in two- and three-dimensions  
 134 to high accuracy and efficiency based on eigenfunction matching. The so-  
 135 lution in three-dimensions was first given by Peter et al. (2004), and the  
 136 solution in two-dimensions was first given by Fox and Squire (1994) for the  
 137 semi-infinite case. Floating elastic plates have been the subject of laboratory  
 138 experiments to validate and show limitations of the model in terms of the  
 139 plate motion (Montiel et al., 2013a,b; Meylan et al., 2015; Yiew et al., 2016)  
 140 and of the scattered wave field (Bennetts et al., 2015; Nelli et al., 2017; Sree  
 141 et al., 2017). While the solution to our problem has appeared previously,  
 142 the simplified numerical solution in two-dimensions given below, which is  
 143 based on symmetry, has not appeared previously to our knowledge. We  
 144 give detailed descriptions to help to understand the computer code which  
 145 accompanies the paper.

146 We begin by stating the governing equations for the floe-water system.  
 147 We assume that the floe has a uniform thickness of  $h$ , the seafloor is flat, and  
 148 that all motions are time-harmonic with radian frequency  $\omega$ . The velocity  
 149 potential in the water,  $\Phi$ , can be expressed as,

$$\Phi(\mathbf{x}, z, t) = \text{Re} \{ \phi(\mathbf{x}, z) e^{-i\omega t} \}, \quad (1)$$

150 where the reduced velocity potential  $\phi$  is complex-valued, and  $\mathbf{x}$  is the hor-  
 151 izontal spatial variable, such that  $\mathbf{x} = x$  in two-dimensions and  $\mathbf{x} = (x, y)$   
 152 in three-dimensions, and  $z$  is the depth variable, which points upwards, with  
 153 the water surface at  $z = 0$  and the seafloor at  $z = -H$ . The ice floe is on  
 154 the free surface ( $z = 0$ ) and occupies the domain  $\Omega$ , where

$$\Omega = \{ \mathbf{x} : |\mathbf{x}| \leq a \}, \quad (2)$$

155  $a$  is the ice floe radius (strictly, in two-dimensions  $2a$  is the ice floe length).

The reduced potential satisfies the boundary value problem

$$\Delta\phi + \partial_z^2\phi = 0, \quad -H < z < 0, \quad (3a)$$

$$\partial_z\phi = 0, \quad z = -H, \quad (3b)$$

$$\partial_z\phi = K\phi, \quad z = 0, \quad \mathbf{x} \notin \Omega, \quad (3c)$$

$$(F\Delta^2 + 1 - K\gamma)\partial_z\phi = K\phi, \quad z = 0, \quad \mathbf{x} \in \Omega, \quad (3d)$$

156 where  $\Delta$  is the Laplacian operator in the horizontal plane. The constant  
 157  $K = \omega^2/g$  is the (deep water) wavenumber, in which  $g \approx 9.81 \text{ m s}^{-2}$  is the  
 158 constant of gravitational acceleration. The parameters  $F$  and  $\gamma$  are non-  
 159 dimensional versions of the flexural rigidity and mass of the floe, respectively,

$$F = \frac{Y h^3}{12(1-\nu^2)\rho g} \quad \text{and} \quad \gamma = \frac{\rho_i h}{\rho}, \quad (3e)$$

160 where  $\rho \approx 1025 \text{ kg m}^{-3}$  is the water density,  $Y \approx 6 \text{ GPa}$  is the Young's  
 161 modulus of sea ice,  $\nu \approx 0.3$  is its Poisson's ratio, and  $\rho_i \approx 925.5 \text{ kg m}^{-3}$  is its  
 162 density (Timco and Weeks, 2010).

163 The floe edges are assumed free, so that the bending moment and shear  
 164 stress vanish. In the two-dimensional problem, the free-edge conditions are

$$\partial_x^2\partial_z\phi = 0, \quad z = 0, \quad |\mathbf{x}| = a, \quad (3f)$$

165

$$\partial_x^3\partial_z\phi = 0, \quad z = 0, \quad |\mathbf{x}| = a. \quad (3g)$$

In three-dimensions, they are

$$\{\Delta - (1-\nu)r^{-1}(\partial_r + r^{-1}\partial_\theta^2)\}\partial_z\phi = 0, \quad z = 0, \quad |\mathbf{x}| = a, \quad (3h)$$

$$\{\partial_r\Delta - (1-\nu)r^{-2}(\partial_r + r^{-1})\partial_\theta^2\}\partial_z\phi = 0, \quad z = 0, \quad |\mathbf{x}| = a, \quad (3i)$$

166 where  $(r, \theta)$  are polar coordinates, such that

$$x = r \cos \theta \quad \text{and} \quad y = r \sin \theta. \quad (4)$$

The vertical eigenfunctions for (3) are

$$\phi_m(z) = \frac{\cos k_m(z + H)}{\cos k_m H}, \quad m = 0, 1, \dots, \quad \mathbf{x} \notin \Omega \quad (5a)$$

$$\text{and} \quad \psi_m(z) = \frac{\cos \kappa_m(z + H)}{\cos \kappa_m H}, \quad m = -2, -1, \dots, \quad \mathbf{x} \in \Omega. \quad (5b)$$

167 The wavenumbers involved in (5) are  $k = k_m$  ( $m = 0, 1, \dots$ ), where

$$k \tan(kH) = -K, \quad (6)$$

168 and  $\kappa = \kappa_m$  ( $m = -2, -1, \dots$ ), where

$$\kappa \tan(\kappa H) = \frac{-K}{F\kappa^4 + 1 - K\gamma}. \quad (7)$$

169 We let  $k_0, \kappa_0 \in i\mathbb{R}_-$ ,  $k_m, \kappa_m \in \mathbb{R}_+$  ( $m = 1, 2, \dots$ ), such that  $k_1 < k_2 < \dots$   
 170 and  $\kappa_1 < \kappa_2 < \dots$ , and  $\kappa_{-2}, \kappa_{-1} \in \mathbb{C}$ , such that  $\kappa_{-1} = -\overline{\kappa_{-2}}$  (in general; for  
 171 details see Bennetts et al., 2007).

172 We note that

$$\int_{-H}^0 \phi_m(z) \phi_n(z) dz = A_m \delta_{mn}, \quad (8)$$

173 where

$$A_m = \frac{1}{2} \left( \frac{\cos k_m H \sin k_m H + k_m H}{k_m \cos^2 k_m H} \right), \quad (9)$$

174 and

$$\int_{-H}^0 \phi_n(z) \psi_m(z) dz = B_{mn}, \quad (10)$$

175 where

$$B_{mn} = \frac{k_n \sin k_n H \cos \kappa_m H - \kappa_m \cos k_n H \sin \kappa_m H}{(\cos k_n H \cos \kappa_m H) (k_n^2 - \kappa_m^2)}. \quad (11)$$



176 Radiation conditions are applied to ensure unique solutions to governing  
 177 equations (3). In two-dimensions, the radiation conditions are

$$\phi(\mathbf{x}, z) \sim \begin{cases} \phi_I(\mathbf{x}, z) + \mathcal{R}\phi_I(-\mathbf{x}, z) & x \rightarrow -\infty, \\ \mathcal{T}\phi_I(\mathbf{x}, z) & x \rightarrow \infty, \end{cases} \quad (12)$$

178 where  $\phi_I(x, z)$  is the incident wave potential

$$\phi_I(\mathbf{x}, z) = e^{ikx}\phi_0(z), \quad (13)$$

179 in which  $k = ik_0$  is the incident wavenumber, and  $\mathcal{R}$  and  $\mathcal{T}$  are the reflection  
 180 and transmission coefficients, respectively. In three-dimensions, the radiation  
 181 condition is

$$\sqrt{r}(\partial_r - ik)(\phi - \phi_I) \rightarrow 0 \quad \text{as } r \rightarrow \infty. \quad (14)$$

### 182 3.1. Solution for two-dimensional model

183 We solve the two-dimensional problem by writing the solution as the  
 184 sum of a symmetric (even) solution,  $\phi^{(s)}(x, z) = \phi^{(s)}(-x, z)$ , and an anti-  
 185 symmetric (odd) solution,  $\phi^{(a)}(x, z) = -\phi^{(a)}(-x, z)$ , which can be solved on  
 186  $x \in (-\infty, 0)$ . This splitting, simplifies the solution to the finite problem and  
 187 makes it a trivial extension of the semi-infinite solution of Fox and Squire  
 188 (1994). To the best of the authors' knowledge, this idea has not appeared in  
 189 the literature previously.

190 Without loss of generality, we assume that the incident potential has unit  
 191 amplitude, and the symmetric solution is given by

$$\phi^{(s)}(x, z) = \phi_I(x, z) + \sum_{m=0}^M a_m^{(s)} e^{k_m(x+a)} \phi_m(z), \quad x < -a, \quad (15)$$

192 in the open water, and

$$\phi^{(s)}(x, z) = \sum_{m=-2}^M b_m^{(s)} \frac{\cosh(\kappa_m x)}{\cosh(\kappa_m a)} \psi_m(z), \quad -a \leq x \leq 0, \quad (16)$$

193 in the ice covered water, for some suitably large  $M$ . To solve for the coeffi-  
 194 cients  $a_m^{(s)}$  ( $m = 0, \dots, M$ ) and  $b_m^{(s)}$  ( $m = -2, \dots, M$ ), we use continuity of  
 195 pressure and horizontal velocity to equate the potential and its derivative at  
 196  $x = -a$ , which gives, respectively,

$$\phi_0(z) + \sum_{m=0}^M a_m^{(s)} \phi_m(z) = \sum_{m=-2}^M b_m^{(s)} \psi_m(z), \quad (17)$$

197 and

$$-k_0 \phi_0(z) + \sum_{m=0}^M a_m^{(s)} k_m \phi_m(z) = - \sum_{m=-2}^M b_m^{(s)} \kappa_m \tanh(\kappa_m h) \psi_m(z). \quad (18)$$

Multiplying both equations by  $\phi_l(z)$  ( $l = 0, \dots, M$ ) and integrating over  
 $z \in (-H, 0)$ , we obtain the system

$$e^{-ika} A_0 \delta_{0l} + a_l^{(s)} A_l = \sum_{m=-2}^M b_m^{(s)} B_{ml}, \quad (19a)$$

$$\text{and} \quad -k_0 e^{-ika} A_0 \delta_{0l} + a_l^{(s)} k_l A_l = - \sum_{m=-2}^M b_m^{(s)} \kappa_m \tanh(\kappa_m a) B_{ml}, \quad (19b)$$

for  $l = 0, 1, \dots, M$ . Applying the free-edge conditions (3e-f) closes the sys-  
 tem with the equations

$$- \sum_{m=-2}^M b_m^{(s)} \kappa_m^3 \tan \kappa_m h = 0, \quad (19c)$$

$$\text{and} \quad \sum_{m=-2}^M b_m^{(s)} \kappa_m^4 \tanh(\kappa_m a) \tan \kappa_m h = 0. \quad (19d)$$

198 The system (19) is solved for the coefficients  $a_m^{(a)}$  ( $m = 0, \dots, M$ ) and  $b_m^{(a)}$   
 199 ( $m = -2, \dots, M$ ).

200 The anti-symmetric solution is found in an almost identical manner. We  
 201 express the solution as

$$\phi^{(a)}(x, z) = \phi_I(x, z) + \sum_{m=0}^M a_m^{(a)} e^{k_m(x+a)} \phi_m(z), \quad x < -a, \quad (20)$$

202 and

$$\phi^{(a)}(x, z) = \sum_{m=-2}^M b_m^{(a)} \frac{\sinh(\kappa_m x)}{\sinh(-\kappa_m a)} \psi_m(z), \quad -a \leq x \leq 0. \quad (21)$$

Applying continuities leads to

$$e^{-ika} A_0 \delta_{0l} + a_l^{(a)} A_l = \sum_{m=-2}^M b_m^{(a)} B_{ml}, \quad (22a)$$

$$\text{and} \quad -\hat{k}_0 e^{-ika} A_0 \delta_{0l} + a_l^{(a)} k_l A_l = - \sum_{m=-2}^M b_m^{(a)} \kappa_m \coth(\kappa_m a) B_{ml}, \quad (22b)$$

for  $l = 0, 1, \dots, M$ , and the free-edge conditions give

$$- \sum_{m=-2}^M b_m^{(a)} \kappa_m^3 \tan \kappa_m h = 0, \quad (22c)$$

$$\text{and} \quad \sum_{m=-2}^M b_m^{(a)} \kappa_m^4 \coth(\kappa_m a) \tan \kappa_m h = 0. \quad (22d)$$

203 The total potential is

$$\phi(x, z) = \frac{1}{2} (\phi^{(s)}(x, z) + \phi^{(a)}(x, z)), \quad (23)$$

and the reflection and transmission coefficients are (from adding the symmetric and anti-symmetric solutions), respectively,

$$\mathcal{R} = \frac{e^{ika}}{2} (a_0^{(s)} + a_0^{(a)}) \quad (24a)$$

$$\text{and} \quad \mathcal{T} = \frac{e^{ika}}{2} (a_0^{(s)} - a_0^{(a)}). \quad (24b)$$

204 *3.2. Solution for three-dimensional model*

205 For circular geometry, the potential can be expressed in terms of cylindrical polar coordinates  $(r, \theta, z)$ , as (Peter et al., 2004)

$$\phi(r, \theta, z) = e^{k_0 x} \phi_0(z) + \sum_{n=-N}^N \sum_{m=0}^M a_{mn} K_n(k_m r) e^{in\theta} \phi_m(z), \quad r > a, \quad (25)$$

207 and

$$\phi(r, \theta, z) = \sum_{n=-N}^N \sum_{m=-2}^M b_{mn} I_n(\kappa_m r) e^{in\theta} \psi_m(z), \quad r < a, \quad (26)$$

for suitably large  $N$  and  $M$ , where  $I_n$  and  $K_n$  are modified Bessel functions,  $a_{mn}$  and  $b_{mn}$  are the coefficients of the potential in the open water and the plate covered region, respectively. We note that

$$\phi_I(\mathbf{x}, z) = \sum_{n=-N}^N I_n(k_0 r) \phi_0(z) e^{in\theta}. \quad (27)$$

As in the solution method for the two-dimensional problems, we use the continuity of potential and its horizontal derivative (radial in this case) across the interface between open and ice-covered water,  $r = a$ . Using orthogonality of the angular (Fourier) modes, we have

$$\begin{aligned} I_n(k_0 a) \phi_0(z) + \sum_{m=0}^M a_{mn} K_n(k_m a) \phi_m(z) \\ = \sum_{m=-2}^{\infty} b_{mn} I_n(\kappa_m a) \psi_m(z) \end{aligned} \quad (28)$$

and

$$\begin{aligned} k_0 I'_n(k_0 a) \phi_0(z) + \sum_{m=0}^M a_{mn} k_m K'_n(k_m a) \phi_m(z) \\ = \sum_{m=-2}^{\infty} b_{mn} \kappa_m I'_n(\kappa_m a) \psi_m(z) \end{aligned} \quad (29)$$

for  $n = -N, \dots, N$ . Multiplying each equations by  $\phi_l(z)$  ( $l = 0, \dots, M$ ) and integrating over  $z \in (-H, 0)$ , from  $-H$  to  $0$ , gives the system

$$I_n(k_0 a) A_0 \delta_{0l} + a_{ln} K_n(k_l a) A_l = \sum_{m=-2}^{\infty} b_{mn} I_n(\kappa_m a) B_{ml} \quad (30)$$

$$k_0 I'_n(k_0 a) A_0 \delta_{0l} + a_{ln} k_l K'_n(k_l a) A_l = \sum_{m=-2}^{\infty} b_{mn} \kappa_m I'_n(\kappa_m a) B_{ml} \quad (31)$$

208 for  $l = 0, 1, \dots, M$  and  $n = -N, \dots, N$ . Equation (30) can be solved for the  
 209 open water coefficients, such that

$$a_{ln} = -\frac{I_n(k_0 a)}{K_n(k_0 a)} \delta_{0l} + \sum_{m=-2}^{\infty} b_{mn} \frac{I_n(\kappa_m a) B_{ml}}{K_n(k_l a) A_l}, \quad (32)$$

for  $l = 0, 1, \dots, M$  and  $n = -N, \dots, N$ , which can then be substituted into  
 equation (31) to give

$$\begin{aligned} & \left( k_0 I'_n(k_0 a) - k_0 \frac{K'_n(k_0 a)}{K_n(k_0 a)} I_n(k_0 a) \right) A_0 \delta_{0l} \\ & = \sum_{m=-2}^{\infty} \left( \kappa_m I'_n(\kappa_m a) - k_l \frac{K'_n(k_l a)}{K_n(k_l a)} I_n(\kappa_m a) \right) B_{ml} b_{mn} \end{aligned} \quad (33)$$

210 for  $l = 0, 1, \dots, M$  and  $n = -N, \dots, N$ .

Free-edge conditions (3g–h) become

$$\sum_{m=-2}^{\infty} \hat{b}_{mn} \left( \kappa_m^2 I_n(\kappa_m a) - \frac{1-\nu}{a} \left( \kappa_m I'_n(\kappa_m a) - \frac{n^2}{a} I_n(\kappa_m a) \right) \right) = 0, \quad (34a)$$

$$\sum_{m=-2}^{\infty} \hat{b}_{mn} \left( \kappa_m^3 I'_n(\kappa_m a) + n^2 \frac{1-\nu}{a^2} \left( \kappa_m I'_n(\kappa_m a) + \frac{1}{a} I_n(\kappa_m a) \right) \right) = 0, \quad (34b)$$

211 for  $n = -N, \dots, N$ , where  $\hat{b}_{mn} = b_{mn} / (F\kappa_m^4 + 1 - K\gamma)$ . Combined with  
 212 equation (33), these conditions give the required equations to solve for the  
 213 coefficients of the water velocity potential in the plate covered region. The  
 214 systems are solved for the different angular modes  $n = 0, 1, \dots, N$  separately,  
 215 noting that the amplitudes for negative values of  $n$  are complex conjugates  
 216 of their positive  $n$  counterparts.

217 The propagating part of the scattered wave is

$$\phi_0(z) = \sum_{n=-N}^N a_{0n} K_n(k_0 r) e^{in\theta} \sim \phi_0(z) r^{-1/2} D(\theta - \theta') e^{ikr} \quad \text{for large } r, \quad (35)$$

218 where

$$D(\theta) = i \sqrt{\frac{\pi}{2k}} \sum_{n=-N}^N a_{0n} e^{in\theta} \quad (36)$$

219 is the far-field amplitude (where  $k = ik_0$  is the incident wavenumber).

220 **4. Wave energy transport in the MIZ**

221 We derive here a simple way to connect the scattering by a single floe with  
 222 attenuation for a large number of floes. We begin with a simplified model  
 223 for wave energy transport in the MIZ, using the model which only considers  
 224 the terms due to ice

$$(\partial_t + \mathbf{c}_g \cdot \nabla) N(\mathbf{x}, t, \theta) = S_{ice}. \quad (37)$$

225 Equation (37) is solved for the wave action density  $N(\mathbf{x}, t, \theta)$ , where  $\theta$  denotes  
 226 wave direction. On the left-hand side of (37),  $\mathbf{c}_g$  is the group velocity, and  
 227  $\nabla = (\partial_x, \partial_y)$  is the gradient operator. The term on the right-hand side,  $S_{ice}$ ,  
 228 is the source term for wave–ice interactions, which, similar to Dumont et al.  
 229 (2011) and Williams et al. (2013a,b), we express as

$$S_{ice} = -c_g a_{ice} \alpha N(\mathbf{x}, t, \theta) \quad \text{where} \quad c_g = |\mathbf{c}_g|, \quad (38)$$

230  $a_{ice}$  is the areal concentration of the ice cover, and  $\alpha$  is the attenuation coef-  
 231 ficient. For simplicity, the chosen form of  $S_{ice}$  neglects nonlinear dissipative  
 232 phenomena, believed to occur during wave–ice interactions in the scattering  
 233 regime, particularly overwash (Skene et al., 2015; Nelli et al., 2020), and  
 234 floe–floe collisions (Shen and Squire, 1998; Bennetts and Williams, 2015;  
 235 Yiew et al., 2017).

236 *4.1. Attenuation coefficient for two-dimensional scattering*

237 For the two-dimensional scattering model, the attenuation coefficient is  
 238 expressed as  $\alpha = \hat{\alpha}/(2a)$ , where  $\hat{\alpha}$  is the attenuation per floe, which is

$$\hat{\alpha} = -\log(|\mathcal{T}|^2), \quad (39)$$

239 where  $|\mathcal{T}|^2$  represents the energy transmitted by an individual floe. The at-  
 240 tenuation coefficient (39) is based on the assumption that all reflected energy

241 is removed from the wave field, which is equivalent to incoherent wave inter-  
 242 actions between the floes. This formula is based on results from scattering  
 243 theory, which show how the scattering from a large number of randomly  
 244 spaced scatterers is connected with individual scattering. Details of this  
 245 derivation can be found in (Bennetts and Squire, 2012). This formula only  
 246 works in two-dimensions. Resonance occurs for certain combinations of wave  
 247 period and floe length, such that  $|T| \approx 1$ , and this leads to unrealistic values  
 248 of the attenuation coefficient,  $\hat{\alpha} = 0$  (Williams et al., 2013a). Therefore, it is  
 249 typical to average the transmitted energy over a distribution of floe lengths,  
 250 so that

$$\hat{\alpha} = -\log(\langle |\mathcal{T}|^2 \rangle), \quad (40)$$

251 where  $\langle \cdot \rangle$  denotes average, which is chosen to be normally distributed with a  
 252 standard deviation  $2a/5$ . The choice of standard deviation is somewhat arbi-  
 253 trary, but the results presented in §5 are largely insensitive to the variations  
 254 in the standard deviation.

#### 255 *4.2. Attenuation coefficient for three-dimensional scattering*

256 For the three-dimensional scattering model, we propose the attenuation  
 257 coefficient is

$$\alpha = \frac{1}{A_f} \int_0^{2\pi} |D(\theta)|^2 d\theta, \quad (41)$$

258 where  $A_f = \pi a^2$  is the area of the ocean surface occupied by an individ-  
 259 ual floe, and the integral is proportional to the energy scattered by the floe  
 260 (Meylan et al., 1997). Attenuation coefficient (41) is based on the assump-  
 261 tion that all scattered energy is removed from the wave field. This is an  
 262 approximation that sets an upper bound on the effect of scattering. More  
 263 complicated scattering models are possible (Meylan et al., 2020).

### 264 4.3. Floe Size Distribution

265 To keep the model simple and easy to implement (and evaluate), the  
266 results we present here, and the accompanying code, assume all floes are  
267 the same size. It would be possible to extend the model to a distribution  
268 of floe sizes by a suitably weighted average of the results calculated here.  
269 This would, of course, also depend on having a suitable floe size distribution.  
270 This is different from the averaging used in the two-dimensional calculations  
271 where the floe size distribution was assumed to be normal.

## 272 5. Results

### 273 5.1. Comparison of two- and three-dimensional attenuation coefficients

274 We present a few representative figures for the attenuation coefficient,  
275 comparing the two and three-dimensional scattering models. We choose the  
276 water depth to be the wavelength of the open water wave to approximate  
277 infinite depth and set  $M = N = 10$  in the expansion formulae. Figure 1  
278 shows the attenuation coefficient as a function of wave period for thickness  
279  $h = 0.5$  m, and for floe radius  $a = 5$  m, 10 m, 25 m and 50 m.

280 The sharp drops in the attenuation coefficient at certain periods for the  
281 two-dimensional case without averaging is caused by resonance. More res-  
282 onances occur as the floe length increases. The resonance is caused by  
283 constructive interference of waves reflected at the ends of the ice floe, anal-  
284 ogous to a Fabry—Perot interferometer. It occurs because waves propagate  
285 through the flexible ice floe. This is a two-dimensional phenomenon and  
286 does not occur for the three-dimensional model in the same simple manner  
287 (since waves are not restricted to travelling in only the forward and backward  
288 direction. The resonances are primarily eliminated by averaging, although  
289 inflexions in the attenuation coefficient still occur at the resonant periods.

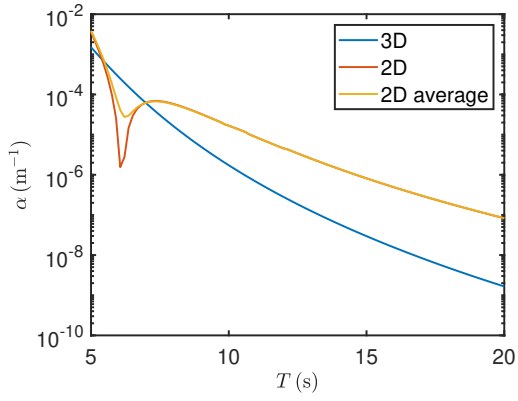


290 We average by sampling with the mean floe length specified and with a  
291 standard deviation one-tenth the mean floe length for our calculations here.  
292 There is some evidence of weak resonance for the three-dimensional case,  
293 with inflexions for the two largest radii. The averaging over angle also helps  
294 to reduce resonant effects in the three-dimensional case. Note that the  
295 resonance occurs at multiples of the wavelength to floe length. As the floes  
296 become larger, there is more possibility for resonances for the wave periods  
297 we consider. There is no simple formula for these resonances because the  
298 wavelength under the ice changes from that of open water, and there is no  
299 simple value for the reflection.

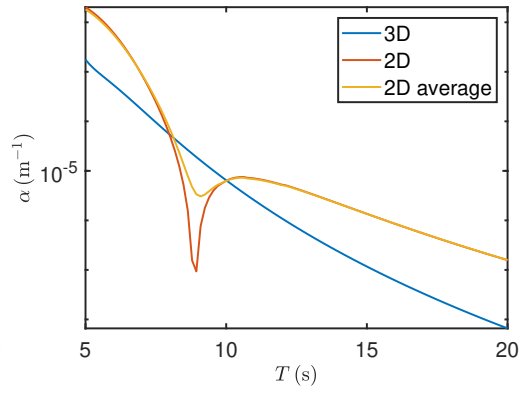
300 Figures 2, 3, and 4 show similar results for floe thickness  $h = 1$  m, 1.5 m,  
301 and 2 m, respectively. Away from resonances, the attenuation coefficient for  
302 the two-dimensional model is higher than the attenuation coefficient for the  
303 three-dimensional model for relatively long periods, i.e. periods correspond-  
304 ing to wavelengths much greater than the floe radius. The difference is up  
305 to two orders of magnitude for long periods and the smallest floes,  $a = 5$  m.  
306 More typically, the two- and three-dimensional scattering models give atten-  
307 uation coefficients of the same order of magnitude, and the three-dimensional  
308 case often exceeds the two-dimensional case for the larger floe radii. From  
309 now on, results for the three-dimensional case only will be considered.

## 310 *5.2. Power laws*

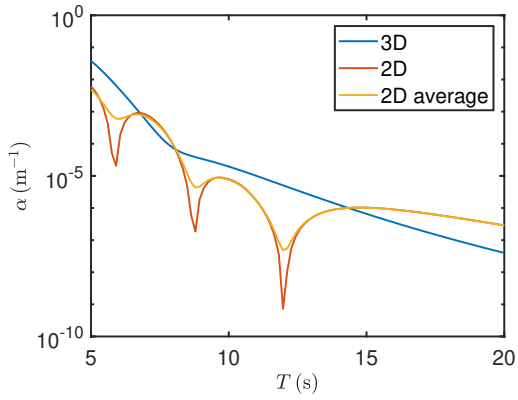
311 Figure 5 shows log-log plots of the attenuation coefficient, as a function  
312 of wave period for different ice thicknesses. For relatively long periods (wave-  
313 lengths greater than the floe radius), the attenuation coefficient versus wave  
314 period is a straight line with a negative slope in log-log space. Therefore, in  
315 the long-period regime, the attenuation coefficient obeys a power law of the



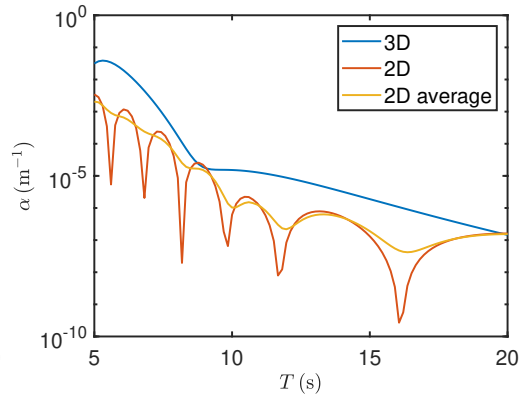
(a) Radius or mean radius  $a = 5$  m



(b) Radius or mean radius  $a = 10$  m

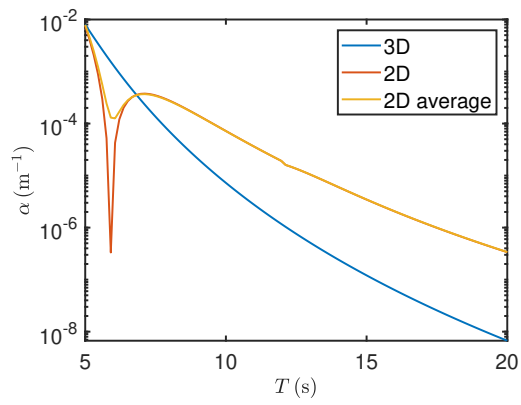


(c) Radius or mean radius  $a = 25$  m

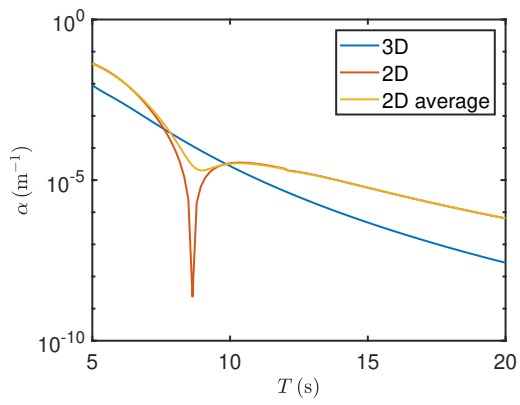


(d) Radius or mean radius  $a = 50$  m

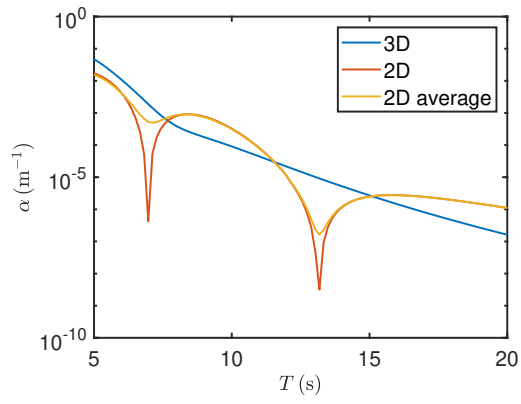
Figure 1: Attenuation  $\alpha$  versus period  $T$  for the two and three dimensional methods for floe thickness  $h = 0.5$  m.



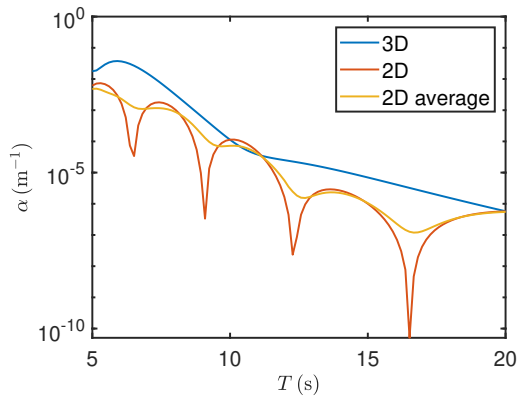
(a) Radius or mean radius  $a = 5$  m



(b) Radius or mean radius  $a = 10$  m

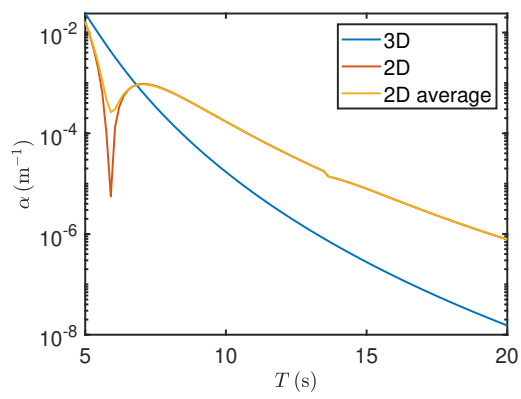


(c) Radius or mean radius  $a = 25$  m

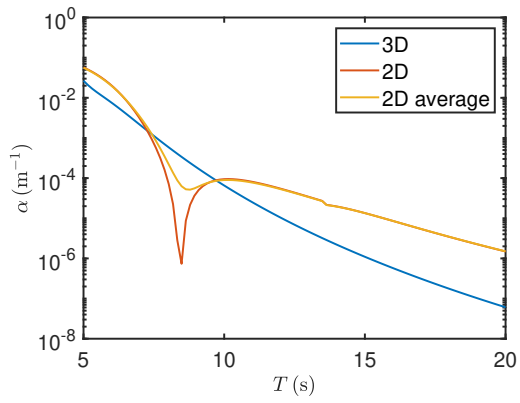


(d) Radius or mean radius  $a = 50$  m

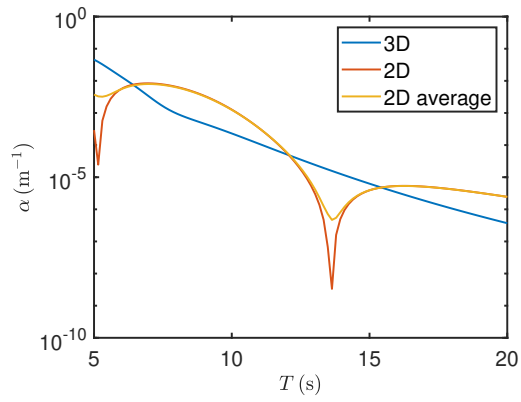
Figure 2: As in Figure 1 except the floe thickness is  $h = 1$  m.



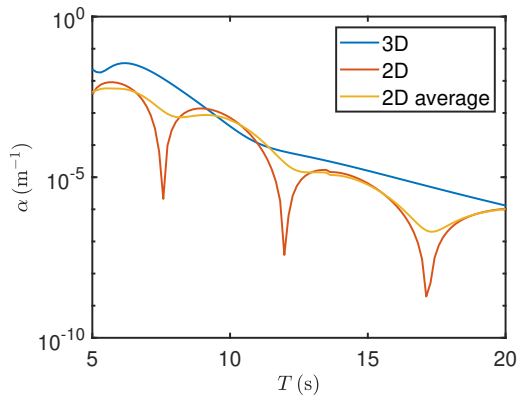
(a) Radius or mean radius  $a = 5$  m



(b) Radius or mean radius  $a = 10$  m

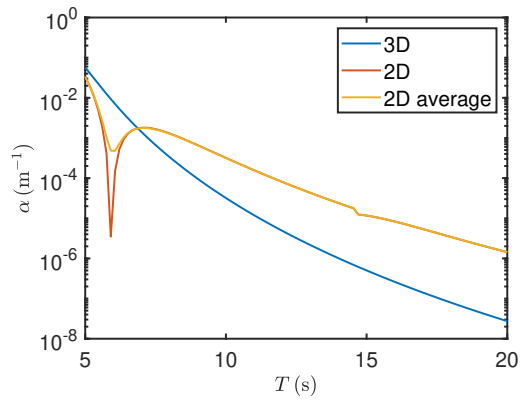


(c) Radius or mean radius  $a = 25$  m

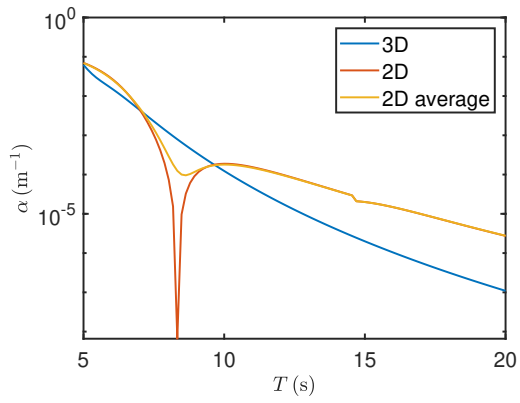


(d) Radius or mean radius  $a = 50$  m

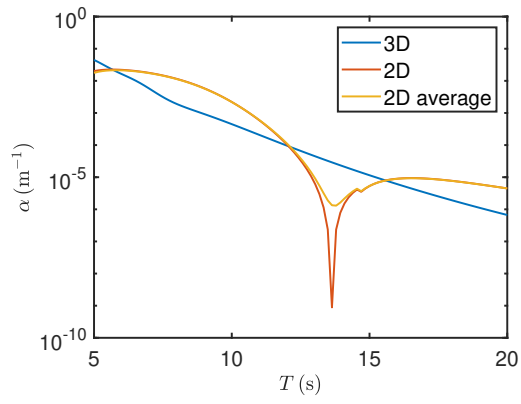
Figure 3: As in Figure 1 except the floe thickness is  $h = 1.5$  m.



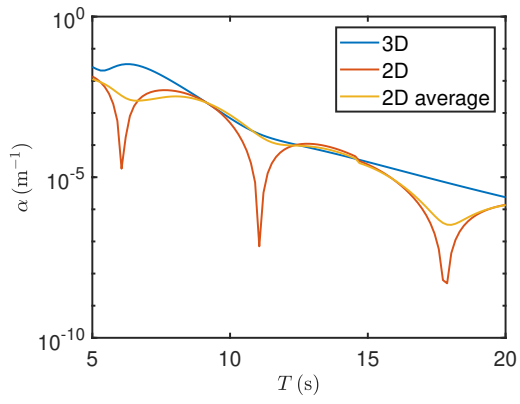
(a) Radius or mean radius  $a = 5$  m



(b) Radius or mean radius  $a = 10$  m



(c) Radius or mean radius  $a = 25$  m



(d) Radius or mean radius  $a = 50$  m

Figure 4: As in Figure 1 except the floe thickness is  $h = 2$  m.

316 form

$$\alpha \propto T^{-p}, \quad (42)$$

317 and the best-fit values of  $p$  for the different thicknesses are shown in the  
318 legends. The value of  $p$  is  $\geq 8$ , which is much greater than the values obtained  
319 from field measurements, i.e.  $p \approx 2$  (Meylan et al., 2014) or 3 (Thomson  
320 et al., 2021).

321 Figure 6 shows log–log plots of the attenuation coefficient as a function  
322 of ice thickness, for different values of wave period and floe radius. For  
323 relatively long periods, the attenuation is a straight line with positive slope,  
324 and therefore

$$\alpha \propto h^q \quad \text{for } T \text{ large.} \quad (43)$$

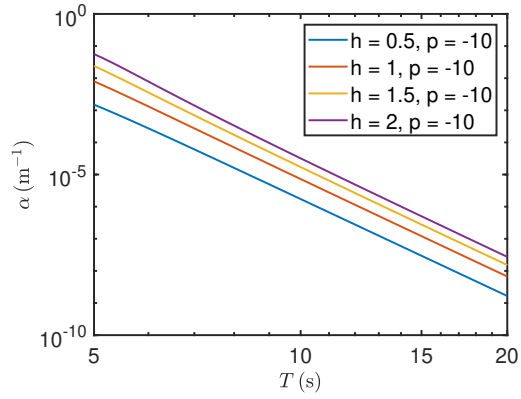
325 The legends show the best-fit values of  $q$ , from which we observe that  $q$  is  
326 generally insensitive to the wave period and floe radius, and  $q \approx 2$ . The  
327 complicated curves for small floes seen in Figure 6 (a) are caused by resonance  
328 effect for rigid floes at short periods, such as a resonant bobbing motion.

### 329 *5.3. Extending the model to heterogeneous distributions of floes.*

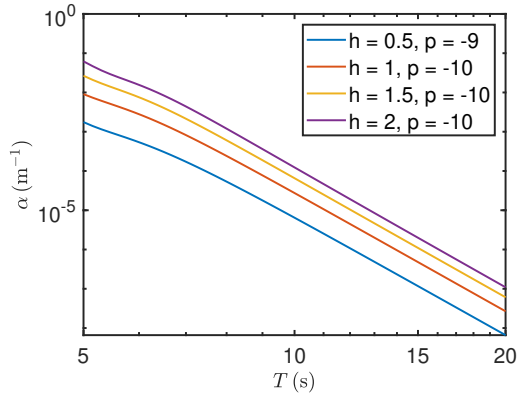
330 A single floe size cannot describe ice floes in the MIZ. It would be possible  
331 to extend the model to the case of floe size distributions by averaging the  
332 effects of each floe size. We do not attempt that here but note that this would  
333 be the logical next step if the scattering model is proven to be suitable.

## 334 **6. Comparison with experiments results**

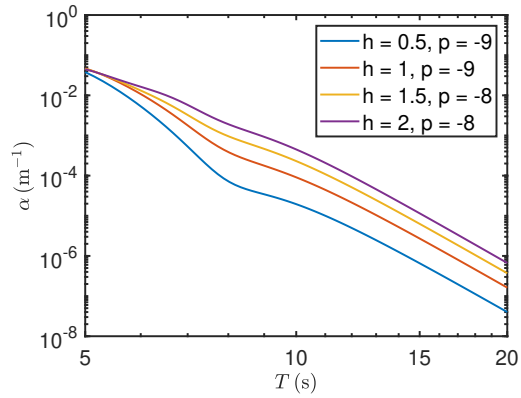
335 Figure 7 shows a comparison of the attenuation coefficient given by the  
336 three-dimensional scattering model, with attenuation coefficient (44), as given  
337 by Meylan et al. (2014). Attenuation due to scattering dominates for short



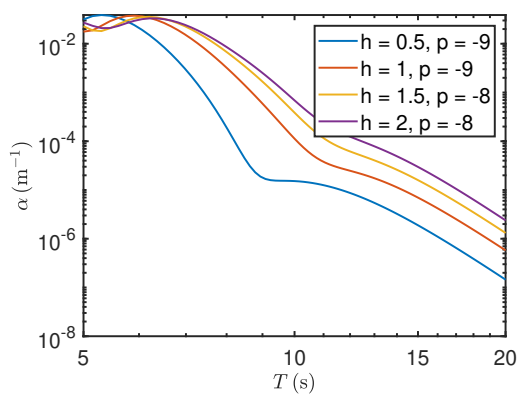
(a) Radius or mean radius  $a = 5$  m



(b) Radius or mean radius  $a = 10$  m



(c) Radius or mean radius  $a = 25$  m



(d) Radius or mean radius  $a = 50$  m

Figure 5: A log-log plot of the attenuation  $\alpha$  as a function of period  $T$  for the thicknesses shown. The coefficient  $T$  is a linear fit in log-log space to give power law relationship in equation (42).

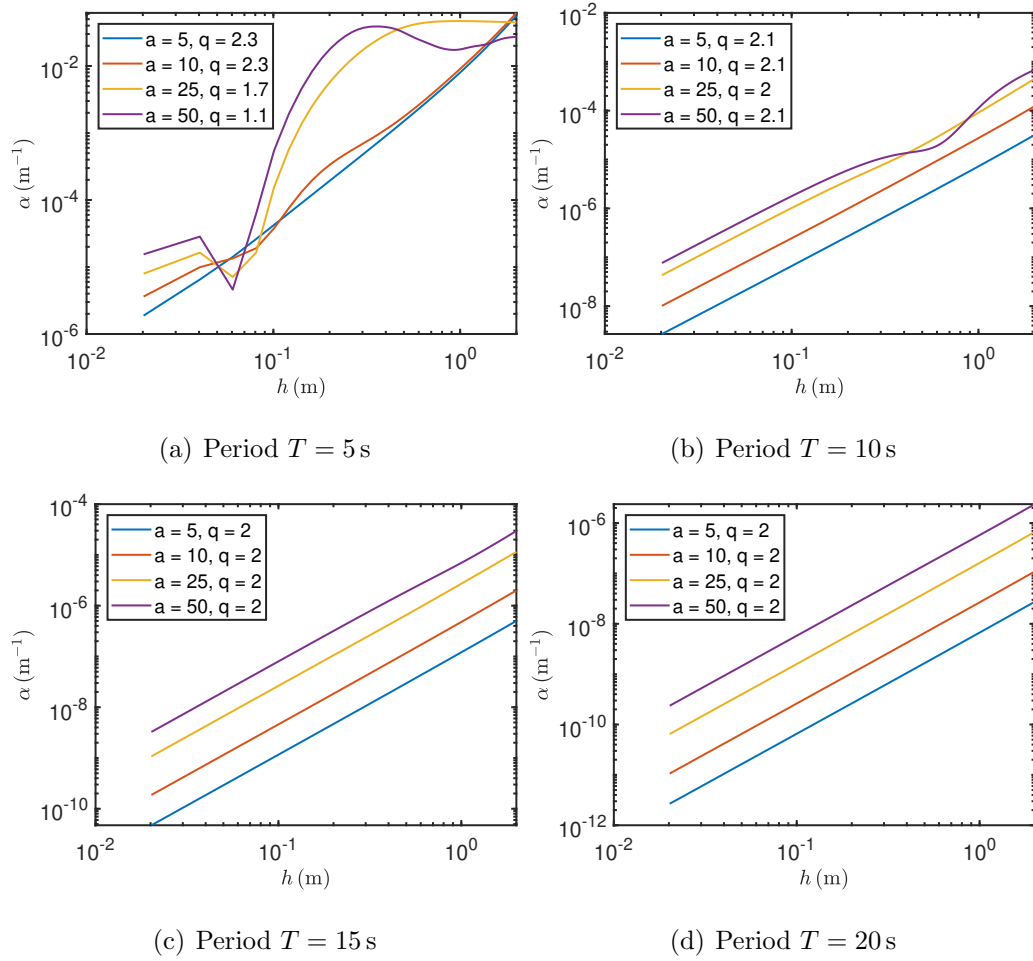


Figure 6: Log–log plot of attenuation coefficient  $\alpha$  as a function of ice thickness  $h$ . The coefficient  $q$  is a linear fit in log–log space to give power law relationship in equation (43)



338 periods, and the empirical attenuation coefficient dominates for long peri-  
339 ods. In field measurements, only long-period attenuation is likely observed  
340 because the scattering attenuation has removed the short periods over a short  
341 distance close to the ice edge.

342 Figure 7 shows a comparison of the attenuation coefficient given by the  
343 three-dimensional scattering model, with experimental data. Figures 7 (a)  
344 shows a comparison with the analysis presented in Rogers et al. (2020) in  
345 which the fitting is based on wave prediction computational code. We believe  
346 this is likely the most accurate experimental results. The four different lines  
347 were based on the sorting of the profiles by their length used in Rogers et al.  
348 (2020). The length is closely related to the wave intensity as a noise floor  
349 cut off was used. We also note that the negative results were discarded so  
350 that a possible upward bias was introduced into the mean values for the  
351 low-intensity cases. The estimated values for the ice thickness was 0.51 m,  
352 0.50 m, 0.47 m, and 0.37 m for the shortest to longest respectively. We run  
353 the comparison with a thickness of 0.5m and a radius of 5m, 10m, and 25m  
354 (assuming concentration is 100%). The agreement with the 25m radius and  
355 the longest results is remarkable. However, we do not claim that this is  
356 sufficient comparison to validate our model or conclusively prove it. We also  
357 note that there is a clear divergence in the attenuation for long periods.

358 Figures 7 (b) shows a comparison with the results first presented in Mey-  
359 lan et al. (2014) but updated with a recent analysis which takes into account  
360 the noise floor of the wave buoys (Thomson et al., 2021). In this case, the  
361 comparison is nowhere near as good and the clear problem for long periods  
362 is apparent. We note that there is no tuning in these results.

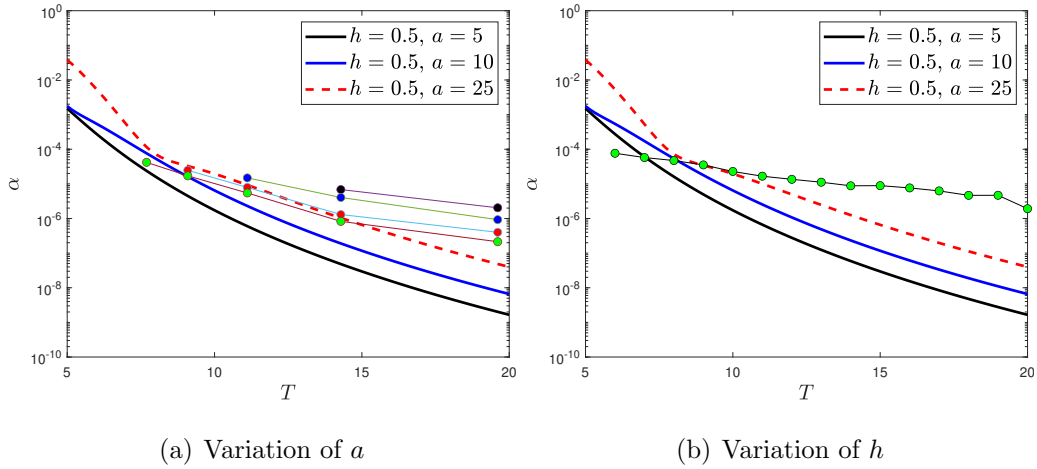


Figure 7: Comparison of attenuation coefficient  $\alpha$  from the three-dimensional scattering model (solid thick lines) with measured attenuation (lines with dots). In (a) the results are from Rogers et al. (2020). The four curves are a sorting based on noise sensitivity. In (b) the comparison is with the measurements of Meylan et al. (2014) with an updated analysis correctly accounting for noise floor (Thomson et al., 2021).

## 363 7. Long-period dissipation

364 It is clear from the comparison with measurements that scattering cannot  
 365 account for the dissipation at long periods. We propose that the attenuation  
 366 due to scattering be augmented by the empirical model

$$\alpha = c_1 T^{-2} + c_2 T^{-4}, \quad (44)$$

367 where  $c_1 = 2.12 \times 10^{-3}$  (s<sup>2</sup>/m) and  $c_2 = 4.59 \times 10^{-2}$  (s<sup>4</sup>/m), which is based on  
 368 measurements reported by Meylan et al. (2014). Note that the coefficients  
 369  $c_1$  and  $c_2$  are likely to depend on the ice conditions, but the dependencies  
 370 have not yet been resolved by measurements or theory. Note also that the  
 371 evidence for the second  $T^{-4}$  term is not as strong as for the first  $T^{-2}$  term.  
 372 We also note that recent evidence (Rogers et al., 2020; Thomson et al., 2021)  
 373 suggest that  $T^{-3}$  may be more appropriate. We also note the numerical  
 374 study of Guyenne and Parau (2017) which supports the idea that for short

375 waves scattering dominates while for long waves it is viscous damping which  
376 dominates.

## 377 8. Summary and discussion

378 Attenuation of waves due to scattering by ice floes has been investigated.  
379 A comparison of the two- and three-dimensional models showed that the  
380 models generally agree in the regime where scattering dominates, notwith-  
381 standing resonances that occur primarily on the two-dimensional model. In  
382 general, it was shown that the three-dimensional model eliminates does not  
383 require need for averaging to eliminate resonances, as in the two-dimensional  
384 model. The long-period asymptotic behaviour of the attenuation coefficient  
385 for the three-dimensional scattering model was shown to be approximately  
386  $T^{-8}$ , i.e. attenuation due to scattering dies out quickly as period increases.  
387 It was deduced that scattering could not account for observed long-period  
388 attenuation, where the exponent has been  $\approx 2$ . We believe this is due to  
389 a viscous damping type model or similar, but note that no model or physi-  
390 cal process has been found which reproduces this behaviour. We, therefore,  
391 propose that the scattering model include an additional parameterised scat-  
392 tering term based on measurements. We have provided the computer code as  
393 supplementary material, and we anticipate that further developments can be  
394 made to it as our understanding advances. We hypothesise that the scattering  
395 model will be necessary during breakup events when the ice cover transitions  
396 from quasi-continuous to a field of relatively small floes. At this point, the  
397 long-period dissipation model will prevail. We note that the key parameters  
398 required for models are the floe thickness and floe size distributions. Both of  
399 these are difficult to measure over large areas of the MIZ

## 400 **Acknowledgements**

401 The authors thank the Isaac Newton Institute for Mathematical Sciences  
402 for support and hospitality during the programme Mathematics of Sea Ice  
403 Phenomena (EPSRC grant number EP/K032208/1), when work on this pa-  
404 per was undertaken, and during which MHM and LGB were supported by  
405 grants from the Simons Foundation. This work is funded by the Australian  
406 Research Council (DP200102828). LGB is supported by an Australian Re-  
407 search Council midcareer fellowship (FT190100404). CH thanks the Na-  
408 tional Institute of Water and Atmospheric Science in New Zealand for their  
409 hospitality and acknowledges support from the Voss Postdoctoral Fellowship  
410 at Brown University and NASA Grant GR5227091.

## 411 **References**

- 412 Alberello, A., Bennetts, L., Heil, P., Eayrs, C., Vichi, M., MacHutchon, K.,  
413 Onorato, M., Toffoli, A., 2020. Drift of pancake ice floes in the winter  
414 antarctic marginal ice zone during polar cyclones. *Journal of Geophysical*  
415 *Research: Oceans* 125 (3), e2019JC015418.
- 416 Ardhuin, F., Otero, M., Merrifield, S., Grouazel, A., Terrill, E., 2020. Ice  
417 breakup controls dissipation of wind waves across southern ocean sea ice.  
418 *Geophys. Res. Lett.* 47 (13), e2020GL087699.
- 419 Ardhuin, F., Sutherland, P., Doble, M., Wadhams, P., 2016. Ocean waves  
420 across the Arctic: Attenuation due to dissipation dominates over scattering  
421 for periods longer than 19 s. *Geophysical Research Letters* 43 (11), 5775–  
422 5783.
- 423 Bateson, A. W., Feltham, D. L., Schröder, D., Hosekova, L., Ridley, J. K.,

- 424 Aksenov, Y., 2020. Impact of sea ice floe size distribution on seasonal  
425 fragmentation and melt of arctic sea ice. *Cryosphere* 14 (2), 403–428.
- 426 Bennetts, L., Alberello, A., Meylan, M., Cavaliere, C., Babanin, A., Toffoli,  
427 A., 2015. An idealised experimental model of ocean surface wave transmis-  
428 sion by an ice floe. *Ocean Model.* 96, 85–92.
- 429 Bennetts, L., Squire, V., 2009. Wave scattering by multiple rows of circular  
430 ice floes. *J. Fluid Mech.* 639, 213–238.
- 431 Bennetts, L., Williams, T., 2010. Wave scattering by ice floes and polynyas  
432 of arbitrary shape. *Journal of Fluid Mechanics* 662, 5–35.
- 433 Bennetts, L., Williams, T., 2015. Water wave transmission by an array of  
434 floating discs. *Proc. R. Soc. A* 471 (2173), 20140698.
- 435 Bennetts, L. G., Biggs, N. R. T., Porter, D., 2007. A multi-mode approxima-  
436 tion to wave scattering by ice sheets of varying thickness. *J. Fluid Mech.*  
437 579, 413–443.
- 438 Bennetts, L. G., O’Farrell, S., Uotila, P., 2017. Impacts of ocean-wave-  
439 induced breakup of Antarctic sea ice via thermodynamics in a stand-alone  
440 version of the CICE sea-ice model. *The Cryosphere* 11 (3), 1035–1040.
- 441 Bennetts, L. G., Peter, M. A., Squire, V. A., Meylan, M. H., 2010. A three-  
442 dimensional model of wave attenuation in the marginal ice zone. *J. Geo-  
443 phys. Res.* 115.
- 444 Bennetts, L. G., Squire, V. A., 2012. On the calculation of an attenua-  
445 tion coefficient for transects of ice-covered ocean. *Proc. Roy. Soc. Lon.*  
446 *A* 468 (2137), 136–162.

- 447 Boutin, G., Ardhuin, F., Dumont, D., Sévigny, C., Girard-Ardhuin, F., Ac-  
448 censi, M., 2018. Floe size effect on wave-ice interactions: Possible effects,  
449 implementation in wave model, and evaluation. *J. Geophys. Res.-Oceans*  
450 123 (7), 4779–4805.
- 451 Boutin, G., Lique, C., Ardhuin, F., Rousset, C., Talandier, C., Accensi, M.,  
452 Girard-Ardhuin, F., 2020. Towards a coupled model to investigate wave–  
453 sea ice interactions in the arctic marginal ice zone. *Cryosphere* 14 (2),  
454 709–735.
- 455 Chen, H., Gilbert, R. P., Guyenne, P., 2019a. Dispersion and attenuation in  
456 a porous viscoelastic model for gravity waves on an ice-covered ocean. *Eur.*  
457 *J. Mech. B-Fluids* 78, 88–105.
- 458 Chen, Z., Bromirski, P., Gerstoft, P., Stephen, R., Lee, W., Yun, S., Olinger,  
459 S., Aster, R., Wiens, D., Nyblade, A. A., 2019b. Ross ice shelf icequakes  
460 associated with ocean gravity wave activity. *Geophysical Research Letters*  
461 46 (15), 8893–8902.
- 462 Cheng, S., Rogers, W. E., Thomson, J., Smith, M., Doble, M. J., Wadhams,  
463 P., Kohout, A. L., Lund, B., Persson, O. P. G., Collins, C. O., Ackley, S.,  
464 Montiel, F., Shen, H. H., 2017. Calibrating a viscoelastic sea ice model for  
465 wave propagation in the Arctic fall marginal ice zone. *J. Geophys. Res.*,  
466 1–24.
- 467 Cheng, S., Stopa, J., Ardhuin, F., Shen, H. H., 2020. Spectral attenuation  
468 of ocean waves in pack ice and its application in calibrating viscoelastic  
469 wave-in-ice models. *Cryosphere* 14 (6), 2053–2069.
- 470 Collins, C. O., Rogers, W. E., Marchenko, A., Babanin, A. V., 2015. In situ

471 measurements of an energetic wave event in the Arctic marginal ice zone.  
472 *Geophys. Res. Lett.* 42 (6), 1863–1870.

473 Doble, M. J., De Carolis, G., Meylan, M. H., Bidlot, J.-R., Wadhams, P.,  
474 2015. Relating wave attenuation to pancake ice thickness, using field mea-  
475 surements and model results. *Geophysical Research Letters* 42 (11), 4473–  
476 4481.

477 Dolatshah, A., Nelli, F., Bennetts, L. G., Alberello, A., Meylan, M. H.,  
478 Monty, J. P., Toffoli, A., 2018. Hydroelastic interactions between water  
479 waves and floating freshwater ice. *Physics of Fluids* 30 (9), 091702.

480 Dumont, D., Kohout, A. L., Bertino, L., 2011. A wave-based model for the  
481 marginal ice zone including a floe breaking parameterization. *J. Geophys.*  
482 *Res.* 116.

483 Fox, C., Squire, V. A., 1994. On the oblique reflexion and transmission of  
484 ocean waves at shore fast sea ice. *Phil. Trans. R. Soc. Lond. A.* 347, 185–  
485 218.

486 Guyenne, P., Parau, E. I., 2017. Numerical simulation of solitary-wave scat-  
487 tering and damping in fragmented sea ice. *Proc. 27th Intl. Ocean Polar*  
488 *Engng Conference*, pp. 373—380.

489 Herman, A., Evers, K.-U., Reimer, N., 2018. Floe-size distributions in labo-  
490 ratory ice broken by waves. *The Cryosphere* 12 (2), 685–699.

491 Horvat, C., Blanchard-Wrigglesworth, E., Petty, A., 2020. Observing waves  
492 in sea ice with icesat-2. *Geophys. Res. Lett.* 47 (10), e2020GL087629.

493 Horvat, C., Tziperman, E., nov 2015. A prognostic model of the sea-ice floe  
494 size and thickness distribution. *Cryosphere* 9 (6), 2119–2134.

- 495 Horvat, C., Tziperman, E., Campin, J.-M., aug 2016. Interaction of sea ice  
496 floe size, ocean eddies, and sea ice melting. *Geophys. Res. Lett.* 43 (15),  
497 8083–8090.  
498 URL <http://doi.wiley.com/10.1002/2016GL069742>
- 499 Keller, J. B., 1998. Gravity waves on ice-covered water. *Journal of Geophys-*  
500 *ical Research: Oceans* 103 (C4), 7663–7669.
- 501 Kohout, A. L., Meylan, M. H., 2008. An elastic plate model for wave at-  
502 tenuation and ice floe breaking in the marginal ice zone. *J. Geophys. Res.*  
503 113 (C9).
- 504 Kohout, A. L., Meylan, M. H., 2009. Wave scattering by multiple floating  
505 elastic plates with spring or hinged boundary conditions. *Mar. Struct.* 22,  
506 712–729.
- 507 Kohout, A. L., Williams, M. J., Dean, S., Meylan, M. H., 2014. Storm-  
508 induced sea ice breakup and the implications for ice extent. *Nature*  
509 509 (7502), 604–607.
- 510 Kohout, A. L., Williams, M. J. M., Toyota, T., Lieser, J., Hutchings, J.,  
511 sep 2016. In situ observations of wave-induced sea ice breakup. *Deep Sea*  
512 *Research Part II: Topical Studies in Oceanography* 131, 22–27.  
513 URL <http://linkinghub.elsevier.com/retrieve/pii/S096706451500212X>
- 514 Liu, A. K., Mollo-Christensen, E., 1988. Wave propagation in a solid ice pack.  
515 *Journal of Physical Oceanography* 18 (11), 1702–1712.
- 516 Massom, R. A., Scambos, T. A., Bennetts, L. G., Reid, P., Squire, V. A.,  
517 Stammerjohn, S. E., 2018. Antarctic ice shelf disintegration triggered by  
518 sea ice loss and ocean swell. *Nature* 558, 383–389.



519 Meylan, M., Bennetts, L., Cavaliere, C., Alberello, A., Toffoli, A., 2015.  
520 Experimental and theoretical models of wave-induced flexure of a sea ice  
521 floe. *Phys. Fluids* 27.

522 Meylan, M. H., 2002. The wave response of ice floes of arbitrary geometry.  
523 *J. Geophys. Res.* 107 (C6).

524 Meylan, M. H., Bennetts, L., 2018. Three-dimensional time-domain scat-  
525 tering of waves in the marginal ice zone. *Philosophical Transactions of*  
526 *the Royal Society A: Mathematical, Physical and Engineering Sciences*  
527 376 (2129), 20170334.

528 Meylan, M. H., Bennetts, L., Mosig, J., Rogers, W., Doble, M., Peter, M. A.,  
529 2018. Dispersion relations, power laws, and energy loss for waves in the  
530 marginal ice zone. *Journal of Geophysical Research: Oceans* 123 (5), 3322–  
531 3335.

532 Meylan, M. H., Bennetts, L. G., Kohout, A. L., 2014. In-situ measurements  
533 and analysis of ocean waves in the antarctic marginal ice zone. *Geophys.*  
534 *Res. Lett.* 41 (14), 5046–5051.

535 Meylan, M. H., Perrie, W., Toulany, B., Hu, Y., Casey, M., 2020. On the  
536 three-dimensional scattering of waves by flexible marginal ice floes. *J Geo-*  
537 *phys. Res.-Oceans* 125 (2).

538 Meylan, M. H., Squire, V. A., 1994. The response of ice floes to ocean waves.  
539 *J. Geophys. Res.* 99 (C1), 891–900.

540 Meylan, M. H., Squire, V. A., Fox, C., 1997. Towards realism in modeling  
541 ocean wave behavior in marginal ice zones. *J. Geophys. Res.* 102 (C10),  
542 22981–22991.

- 543 Montiel, F., Bennetts, L. G., Squire, V. A., Bonnefoy, F., Ferrant, P., 2013a.  
544 Hydroelastic response of floating elastic discs to regular waves. Part 1.  
545 Wave basin experiments. *J. Fluid Mech.* 723, 604–628.
- 546 Montiel, F., Bennetts, L. G., Squire, V. A., Bonnefoy, F., Ferrant, P., 2013b.  
547 Hydroelastic response of floating elastic discs to regular waves. Part 2.  
548 Modal analysis. *J. Fluid Mech.* 723, 629–652.
- 549 Montiel, F., Squire, V., Bennetts, L., 2016. Attenuation and directional  
550 spreading of ocean wave spectra in the marginal ice zone. *J. Fluid Mech.*  
551 790, 492–522.
- 552 Mosig, J. E. M., Montiel, F., Squire, V. A., 2015. Comparison of viscoelastic-  
553 type models for ocean wave attenuation in ice-covered seas. *Journal of*  
554 *Geophysical Research: Oceans* 120 (9), 6072–6090.  
555 URL <http://dx.doi.org/10.1002/2015JC010881>  
556 <http://doi.wiley.com/10.1002/2015JC010881>
- 557 Nelli, F., Bennetts, L., Skene, D., Monty, J., Lee, J., Meylan, M., Toffoli,  
558 A., 2017. Reflection and transmission of regular water waves by a thin,  
559 floating plate. *Wave Motion* 70, 209–221.
- 560 Nelli, F., Bennetts, L. G., Skene, D. M., Toffoli, A., 2020. Water wave trans-  
561 mission and energy dissipation by a floating plate in the presence of over-  
562 wash. *J. Fluid Mech.* 889.
- 563 Perrie, W., Hu, Y., 1996. Air–ice–ocean momentum exchange. part 1:energy  
564 transfer between waves and ice floes. *J. of Phys. Ocean.* 26, 1705–1720.
- 565 Peter, M. A., Meylan, M. H., 2009. Water-wave scattering by vast fields of  
566 bodies. *SIAM J. Appl. Math.* 70 (5), 1567–1586.

- 567 Peter, M. A., Meylan, M. H., Chung, H., 2004. Wave scattering by a circular  
568 elastic plate in water of finite depth: a closed form solution. *Int. J. Offshore*  
569 *Polar* 14 (2), 81–85.
- 570 Rabault, J., Sutherland, G., Gundersen, O., Jensen, A., Marchenko, A.,  
571 Breivik, Ø., 2020. An open source, versatile, affordable waves in ice in-  
572 strument for scientific measurements in the polar regions. *Cold Reg. Sci.*  
573 *Techol.* 170, 102955.
- 574 Roach, L. A., Bitz, C. M., Horvat, C., Dean, S. M., dec 2019. Advances in  
575 Modeling Interactions Between Sea Ice and Ocean Surface Waves. *Journal*  
576 *of Advances in Modeling Earth Systems* 11 (12), 4167–4181.  
577 URL <https://onlinelibrary.wiley.com/doi/abs/10.1029/2019MS001836>
- 578 Roach, L. A., Horvat, C., Dean, S. M., Bitz, C. M., 2018. An emergent sea ice  
579 floe size distribution in a global coupled ocean-sea ice model. *J. Geophys.*  
580 *Res.-Oceans* 123 (6), 4322–4337.
- 581 Rogers, E. W., Meylan, M. H., Kohout, A. L., 2020. Estimates of spectral  
582 wave attenuation in antarctic sea ice, using model/data inversion. *Cold*  
583 *Reg. Sci. and Tech.*, 103198.
- 584 Rogers, W. E., Thomson, J., Shen, H. H., Doble, M. J., Wadhams, P., Cheng,  
585 S., 2016. Dissipation of wind waves by pancake and frazil ice in the autumn  
586 b eaufort s ea. *J. Geophys. Res.-Oceans* 121 (11), 7991–8007.
- 587 Shen, H. H., Squire, V. A., 1998. Wave Damping in Compact Pancake Ice  
588 Fields Due to Interactions Between Pancakes. In: Jeffries, M. O. (Ed.),  
589 *Antarctic Research Series*. American Geophysical Union, Washington, D.  
590 C., pp. 325–341.

- 591 Skene, D., Bennetts, L., Meylan, M., Toffoli, A., 2015. Modelling water wave  
592 overwash of a thin floating plate. *Journal of Fluid Mechanics* 777, R3.
- 593 Squire, V., Moore, S. C., 1980. Direct measurement of the attenuation of  
594 ocean waves by pack ice. *Nature* 283 (5745), 365 – 368.
- 595 Squire, V. A., 2020. Ocean wave interactions with sea ice: a reappraisal.  
596 *Annu. Rev. Fluid Mech.* 52, 37–60.
- 597 Sree, D. K. K., Law, A. W.-K., Shen, H. H., 2017. An experimental study  
598 on the interactions between surface waves and floating viscoelastic covers.  
599 *Wave Motion* 70, 195–208.
- 600 Sutherland, G., Rabault, J., Christensen, K. H., Jensen, A., 2019. A two  
601 layer model for wave dissipation in sea ice. *Appl. Ocean Res.* 88, 111–118.
- 602 Sutherland, P., Brozena, J., Rogers, W. E., Doble, M., Wadhams, P., 2018.  
603 Airborne remote sensing of wave propagation in the marginal ice zone. *J.*  
604 *Geophys. Res.-Oceans* 123 (6), 4132–4152.
- 605 Thomson, J., Ackley, S., Girard-Ardhuin, F., Ardhuin, F., Babanin, A.,  
606 Boutin, G., Brozena, J., Cheng, S., Collins, C., Doble, M., et al., 2018.  
607 Overview of the arctic sea state and boundary layer physics program. *J*  
608 *Geophys. Res.-Oceans* 123 (12), 8674–8687.
- 609 Thomson, J., Hosekova, L., Meylan, M. H., Kohout, A. L., Kumar, N., 2021.  
610 Spurious rollover of wave attenuation rates in sea ice caused by noise in  
611 field measurements. *J Geophys. Res.-Oceans*.
- 612 Timco, G., Weeks, W., 2010. A review of the engineering properties of sea  
613 ice. *Cold Reg. Sci. Technol.* 60 (2), 107–129.

- 614 Toffoli, A., Bennetts, L. G., Meylan, M. H., Cavaliere, C., Alberello, A.,  
615 Elsnab, J., Monty, J. P., 2015. Sea ice floes dissipate the energy of steep  
616 ocean waves. *Geophys. Res. Lett.* 42 (20), 8547–8554.
- 617 Voermans, J., Babanin, A., Thomson, J., Smith, M., Shen, H., 2019. Wave  
618 attenuation by sea ice turbulence. *Geophys. Res. Lett.* 46 (12), 6796–6803.
- 619 Wadhams, P., Squire, V. A., Goodman, D. J., Cowan, A. M., Moore, S. C.,  
620 1988. The attenuation rates of ocean waves in the marginal ice zone. *J.*  
621 *Geophys. Res.* 93 (C6), 6799 – 6818.
- 622 Wang, R., Shen, H. H., 2010a. Gravity waves propagating into an ice-covered  
623 ocean: A viscoelastic model. *Journal of Geophysical Research* 115 (C6),  
624 C06024.  
625 URL <http://dx.doi.org/10.1029/2009JC005591>  
626 <http://doi.wiley.com/10.1029/2009JC005591>
- 627 Wang, R., Shen, H. H., 2010b. Gravity waves propagating into an ice-covered  
628 ocean: A viscoelastic model. *J. Geophys. Res.* 115 (C6).
- 629 Weber, J. E., 1987. Wave attenuation and wave drift in the marginal ice zone.  
630 *J. Phys. Oceanogr.* 17 (12), 2351–2361.
- 631 Williams, T. D., Bennetts, L. G., Squire, V. A., Dumont, D., Bertino, L.,  
632 2013a. Wave–ice interactions in the marginal ice zone. Part 1: Theoretical  
633 foundations. *Ocean Model.* 71, 81–91.
- 634 Williams, T. D., Bennetts, L. G., Squire, V. A., Dumont, D., Bertino, L.,  
635 2013b. Wave–ice interactions in the marginal ice zone. Part 2: Numerical  
636 implementation and sensitivity studies along 1D transects of the ocean  
637 surface. *Ocean Model.* 71, 92–101.

- 638 Williams, T. D., Rampal, P., Bouillon, S., 2017. Wave-ice interactions in the  
639 neXtSIM sea-ice model. *The Cryosphere* 11 (5), 2117–2135.
- 640 Yiew, L. J., Bennetts, L. G., Meylan, M. H., French, B. J., Thomas, G. A.,  
641 2016. Hydrodynamic responses of a thin floating disk to regular waves.  
642 *Ocean Model.* 97, 52–64.
- 643 Yiew, L. J., Bennetts, L. G., Meylan, M. H., Thomas, G. A., French, B. J.,  
644 2017. Wave-induced collisions of thin floating disks. *Physics of Fluids*  
645 29 (12), 127102.
- 646 Zhang, J., Stern, H., Hwang, B., Schweiger, A., Steele, M., Stark, M., Graber,  
647 H. C., 2016. Modeling the seasonal evolution of the Arctic sea ice floe size  
648 distribution. *Elem Sci Anth* 4, 000126.